Chinese Chemical Letters 35 (2024) 108672

Contents lists available at ScienceDirect

Chinese Chemical Letters

journal homepage: www.elsevier.com/locate/cclet

Tumor microenvironment-activatable neuropeptide-drug conjugates enhanced tumor penetration and inhibition *via* multiple delivery pathways and calcium deposition

Yi Cao[a,b,c], Xiaojiao Ge[a,c], Yuanyuan Wei[a,c], Lulu He[a,c], Aiguo Wu[a,c,*], Juan Li[a,c,*]

[a] *Ningbo Key Laboratory of Biomedical Imaging Probe Materials and Technology, Zhejiang International Cooperation Base of Biomedical Materials Technology and Application, Chinese Academy of Sciences (CAS) Key Laboratory of Magnetic Materials and Devices, Ningbo Cixi Institute of Biomedical Engineering, Zhejiang Engineering Research Center for Biomedical Materials, Ningbo Institute of Materials Technology and Engineering, Chinese Academy of Sciences, Ningbo 315201, China*

[b] *University of Chinese Academy of Sciences, Beijing 100049, China*

[c] *Advanced Energy Science and Technology Guangdong Laboratory, Huizhou 516000, China*

ARTICLE INFO

Article history:
Received 9 March 2023
Revised 31 May 2023
Accepted 8 June 2023
Available online 9 June 2023

Keywords:
Neuropeptide-drug conjugate
Tumor penetration
Calcium deposition
Tumor inhibition
Triple-negative breast cancer

ABSTRACT

Peptide-drug conjugates have achieved considerable development and application as a novel strategy for targeted delivery of anticancer drugs. Bioactive peptides induced calcium deposition can irreversibly assist inhibition of tumors. However, active regulation of calcium level through signal transduction of bioactive substances has not been reported yet. In this study, novel neuropeptide-doxorubicin conjugates (NP-DOX) with lysosome-specific acid response were described for neuropeptide Y_1 receptor (Y_1R)-overexpressed triple-negative breast cancer. The delivery mechanism of NP-DOX was clarified that diverse pathways were involved, including intracellular and intercellular transport. Importantly, up-regulation of Y_1R-mediated intracellular calcium level *via* second messenger inositol triphosphate was presented in NP-DOX treated MDA-MB-231 cells. *In vivo* antitumor efficacy demonstrated that NP-DOX showed less organ toxicity and enhanced tumor inhibition benefited from its controlled release and Y_1R-mediated calcium deposition, compared with free DOX. This bioconjugate is a proof-of-concept confirming that neuropeptide-mediated control of signaling responses in neuropeptide-drug conjugates enables great potential for further applications in tumor chemotherapy.

Neuropeptides, as a class of peptide hormone, have a critical impact on the regulation of neuronal activity, food intake, energy homeostasis and even cancer progression [1–3]. Based on the high expression of neuropeptide receptors in tumor, neuropeptides as targeting motifs have been utilized for construction of neuropeptide-drug conjugates, which made significant progress in targeted and personalized cancer treatment [4–6]. As one of the most abundant neuropeptides, neuropeptide Y (NPY) has been identified as a paracrine factor secreted by cancer cells that acts as an independent regulator of cancer angiogenesis [7]. Up to now, various tumors have identified susceptible to neuropeptide Y receptors (NPYRs) signaling, which can lead to possible outcomes including the stimulation of tumor development, prevention of tumor growth, and activation of apoptosis [8–11]. Thus, NPYRs might be the most promising strategy for cancer targeting [12,13]. However, some challenges remained that inefficient tumor inhibition was obtained due to low efficiency of tumor cell internalization, uncontrollable drug release, monotonous pathway of drug delivery and traditional medicine-dependent mechanism of drug action [14,15]. Thus, novel functionally integrated neuropeptide-drug conjugates are urgently needed to explore for improved drug delivery.

In addition, NPYRs belong to G protein-coupled receptors (GPCRs), who can regulate the activity of ion channels through second messenger systems as the largest family of hormone and neurotransmitter receptors on cell membranes [16,17]. Calcium is one of the most crucial second messengers and plays an important role in controlling the occurrence and development of tumors. Tumor calcification is regarded as a process of tumor apoptosis [18]. In recent years, this irreversible destructive process has become a novel strategy applicable to cancer treatment. The early efforts have been focused on construction and delivery of exogenous calcium to passively trigger this biomineralization process [19–22]. However, abnormally high local concentrations of calcium can trigger a

* Corresponding authors.
E-mail addresses: aiguo@nimte.ac.cn (A. Wu), lij@nimte.ac.cn (J. Li).

https://doi.org/10.1016/j.cclet.2023.108672
1001-8417/

hypercalcemic crisis, leading to serious conditions such as cardiac arrest, necrotizing pancreatitis, kidney failure and even death. Recently, folate-, peptide-, or phosphorylated polymer-based calcium binding in tumor tissues has been reported [23–27]. These negative-charged groups served as biomineralization-inducing sites to recruit positive ions, mainly calcium ion, leading to the necessary of intervention of carriers for tumor targeting or tumor microenvironment response [28]. So far, active regulation of calcium level through signal transduction of bioactive substances is rarely studied. On this basis, neuropeptide-mediated calcium regulation may be a new direction to break through.

Herein, acid-activatable conjugate neuropeptide-doxorubicin conjugates (NP-DOX) based on NPY was provided for effective delivery to Y_1 receptor (Y_1R) over-expressed triple-negative breast cancer (TNBC). To begin with, endocytosis mechanism of NP-DOX in MDA-MB-231 cells was systematically clarified, which was mainly mediated by clathrin, Y_1R, and micropinocytosis. Subsequently, a portion of NP-DOX was delivered to lysosomes, where acid-responsive drug activation was conducted to convert NP-DOX to free DOX. NP-DOX not captured by lysosomes was exocytosed and internalized *via* transcytosis, enabling intercellular migration to achieve deep penetration for drug delivery. Most importantly, NP-DOX induced promotion of intracellular calcium level *via* second messenger inositol triphosphate (IP3) was observed, revealing Y_1R-mediated calcium regulation in MDA-MB-231 cells. Compared with free DOX, NP-DOX appeared to have less toxicity toward the heart and spleen and significantly suppressed tumor growth after treatment. Massive calcium deposition was detected in NP-DOX treated tumor tissues, which indicated Y_1R-mediated calcium overload-enhanced chemotherapy. From this, multiple biological functionally integrated conjugates have great potential for further application in tumor chemotherapy.

Tumor microenvironment-activatable neuropeptide drug conjugate NP-DOX was designed by linking NPY analogue [Asn^{28}, Pro^{30}, Trp^{32}]-NPY (25–36) (sequence: NH_2-RHYNNPIWRQRY-NH_2, abbreviated as P12) to the prescribed cytotoxin DOX *via* an acid-sensitive hydrazone bond, in which P12 was requisitioned for Y_1R up-regulated TNBC tumor targeting. The synthesis of NP-DOX was illustrated in Fig. S1 (Supporting information) and the obtained NP-DOX was identified by high performance liquid chromatograph (HPLC) and quadrupole time-of-flight (Q-TOF) mass spectrometry. As exemplarily shown in Figs. 1A and B, the peak generated at 5.2 min in HPLC spectrum and $[M+2H]^{2+}$ signals displayed in positive electrospray ionization (ESI+) mass spectrum suggested the successful synthesis of NP-DOX. The absorption spectrum of NP-DOX in Fig. S2 (Supporting information) contained the characteristic absorption peak of DOX at 480 nm. To get the concentration of NP-DOX successfully estimated, the concentration-absorbance standard curves of NP-DOX was plotted.

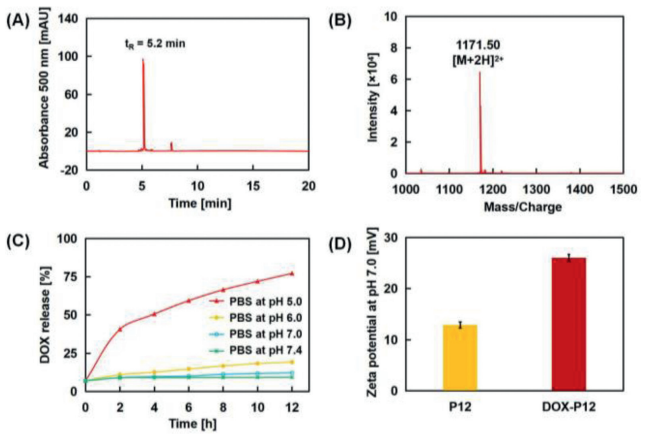

Fig. 1. Analytical data of NP-DOX. (A) Analytical HPLC spectrum of NP-DOX. (B) ESI+ mass spectra of NP-DOX. (C) DOX release from NP-DOX in PBS with different pH values at indicated time *via* HPLC analysis. (D) Zeta potential of P12 and NP-DOX at pH 7.0. Data are presented as means ± standard deviations (n=3).

The pH-dependent DOX release from NP-DOX was analyzed by HPLC at the wavelength of 500 nm as described before. As shown in Fig. 1C, only a slight portion (less than 10%) of NP-DOX was hydrolyzed to DOX even over a long period of 12 h in phosphate buffer solution (PBS) with pH 7.4. As pH decreased, DOX release at pH 7.0 and 6.0 got a slight increase to 12% and 19%, respectively. Notably, the accumulated DOX release in 12 h reached 77% at pH 5.0 PBS environment, achieving acid-activatable DOX release.

Positive charge-induced transcytosis has been proposed for enhanced drug delivery and tumor penetration [29–31]. NPY is a 36-amino acid peptide, whose isoelectric point is close to physiological pH. Thus, NPY was almost uncharged as calculated based on Lehninger Principles of Biochemistry (Table S1 in Supporting information), from which, positively charged P12 was designed *via* sequence truncation and mutation. Zeta potentials of P12 and NP-DOX at pH 7.0 were measured in Fig. 1D. The results confirmed the positive charge of P12 and NP-DOX, and more positive charges in NP-DOX, which might be related to the protonation of amino group on DOX in pH 7.0.

Generally speaking, the endocytosis pathways can be divided into macropinocytosis, clathrin-mediated, caveolin-mediated, and clathrin/caveolin-independent endocytosis. It is reported that clathrin-mediated endocytosis will eventually undergo lysosomal destruction, while caveolin-mediated and macropinocytosis pathways can prevent or minimize the carrier entering lysosomes [32,33]. Therefore, the internalization mechanism of drugs is very important in the early stage of transcytosis [34,35]. To reveal the endocytosis mechanism of NP-DOX, five endocytosis inhibitors (chloroquine, BIBO3304, chlorpromazine, amiloride, and methyl-β-cyclodextrin) were employed. As investigated in Fig. S4 (Supporting information), chlorpromazine (clathrin-mediated endocytosis inhibitor), BIBO3304 (Y_1R antagonist), and amiloride (macropinocytosis inhibitor) decreased the cellular uptake of NP-DOX by 32%, 23%, and 9%, respectively, which indicated multiple pathways involved in the endocytosis process of NP-DOX in MDA-MB-231 cells. These results contributed from not only the cationization of NP-DOX, but also the affinity to Y_1R. When a large amount of NP-DOX accumulated outside the cells, the binding of NP-DOX to Y_1R reached saturation very quickly. At the same time, clathrin-mediated endocytosis was dominant as main endocytosis pathway for the vast majority of cells. Moreover, macropinocytosis also participated in transporting NP-DOX as a nonselective endocytic route. Integrating the above pathways, NP-DOX achieved rapid cell internalization in a short period of time.

To investigate the distribution of NP-DOX after being endocytosed, intracellular location of NP-DOX after 30 min and 1 h was captured by confocal laser scanning microscopy (CLSM). As Fig. 2A recorded, a proportion of NP-DOX was situated in lysosome 30 min after internalization, where NP-DOX could be acid-responsively activated to release DOX. After another 30 min, DOX derived from NP-DOX was almost delivered to the nucleus. Compared with the fast passive distribution of DOX in the nucleus, the active selectively drug release and progressive drug delivery of NP-DOX was much more intelligent for tumor chemotherapy, expected to achieve better therapeutic effect and minimize systemic toxicity.

Nonspecific membrane toxicity is considered main crucial barrier for application of cell-penetrating peptide. To evaluate toxic profile of P12, hemolysis assay was carried out. As shown in Fig. S5 (Supporting information), rarely low hemolytic activity of P12 was detected even at 25 mg/mL, demonstrating relatively low membrane toxicity. Further, cell cytotoxicity assessment of NP-DOX was

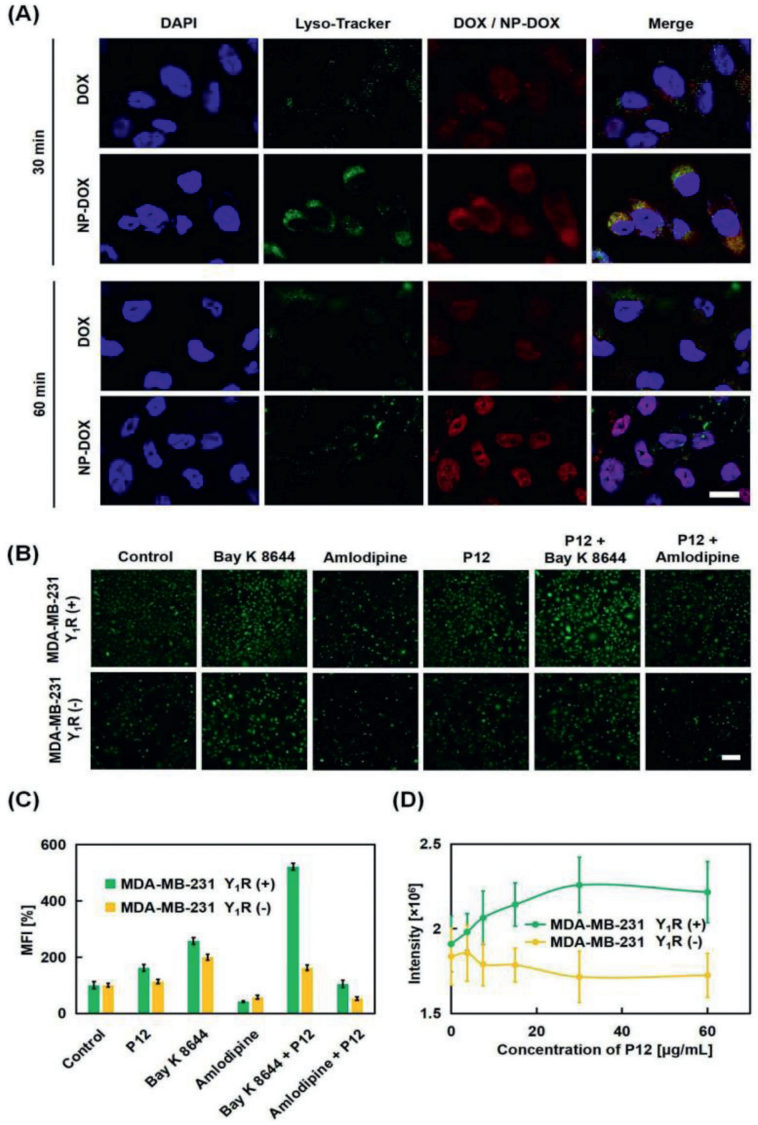

Fig. 2. Study on intracellular location and calcium response of NP-DOX in MDA-MB-231. (A) CLSM images of MDA-MB-231 cells incubated with NP-DOX after 30 and 60 min. Scale bar = 20 μm. (B) Fluorescence images and (C) analyzed mean fluorescence intensity (MFI) of calcium probe in MDA-MB-231 and Y_1R-knock-down MDA-MB-231 cells with P12, Bay K 8644 (calcium channel agonist), and amlodipine (calcium channel blocker) treated. (D) Fluorescence intensity of P12-treated MDA-MB-231 cells with a series of concentrations of P12 from 3.75 μg/mL to 60 μg/mL. Scale bar = 200 μm. Data are presented as means ± standard deviations ($n = 3$).

carried out in MDA-MB-231 cells with NP-NHCO-DOX as a non-releasable system (Fig. S6 in Supporting information). The results in Figs. S7 and S8 (Supporting information) revealed that the cell viability was strongly inhibited due to the design of cleavable linker in NP-DOX after 24 h incubation with a half maximal inhibitory concentration (IC_{50}) of 4 μg/mL, nearly 100-fold lower than that of NP-NHCO-DOX. The IC_{50} of NP-DOX at 48 h was close to that of free DOX at 24 h (Table 1). Overall, NP-DOX exhibited evidently time-dependent cytotoxicity towards MDA-MB-231 cells.

Table 1
Mean IC_{50} values of free DOX, NP-DOX, and NP-NHCO-DOX on MDA-MB-231 cells after 24, 36, and 48 h incubation.

Group	IC_{50} (μg/mL)		
	DOX	NP-DOX	NP-NHCO-DOX
24 h	0.2	4.0	373.1
36 h	ND	1.7	115.8
48 h	ND	0.5	52.3

According to the results of endocytosis study and intracellular distribution, the inhibition may come from acid-responsive activation of more than 32% NP-DOX (clathrin- and Y_1R-mediated endocytosis) to release DOX in lysosomes.

Despite the cleavable linker greatly aided in cell inhibition, the potential influence of Y_1R was further discovered in Fig. 2B. It has been reported the binding of NPY and its receptors will alter free intracellular calcium concentrations. Thus, calcium level of MDA-MB-231 cells and Y_1R-knock-down MDA-MB-231 cells (Fig. S9 in Supporting information) were studied using the fluorescent calcium-indicator among five treated groups (3 μg/mL P12, 100 ng/mL Bay K 8644, 30 μg/mL amlodipine, 3 μg/mL P12 + 100 ng/mL Bay K 8644, and 3 μg/mL P12 + 30 μg/mL amlodipine). The varying fluorescence intensities in Figs. 2C and D revealed Y_1R-mediated promotion on calcium level of P12 in MDA-MB-231 cells, which may result in calcium overload to trigger an enhanced inhibition of cancer cells.

To identify the mechanisms in the up-regulation of calcium level after activation of NPYRs, a lot of second messengers have been investigated in the last century, among which, generation of

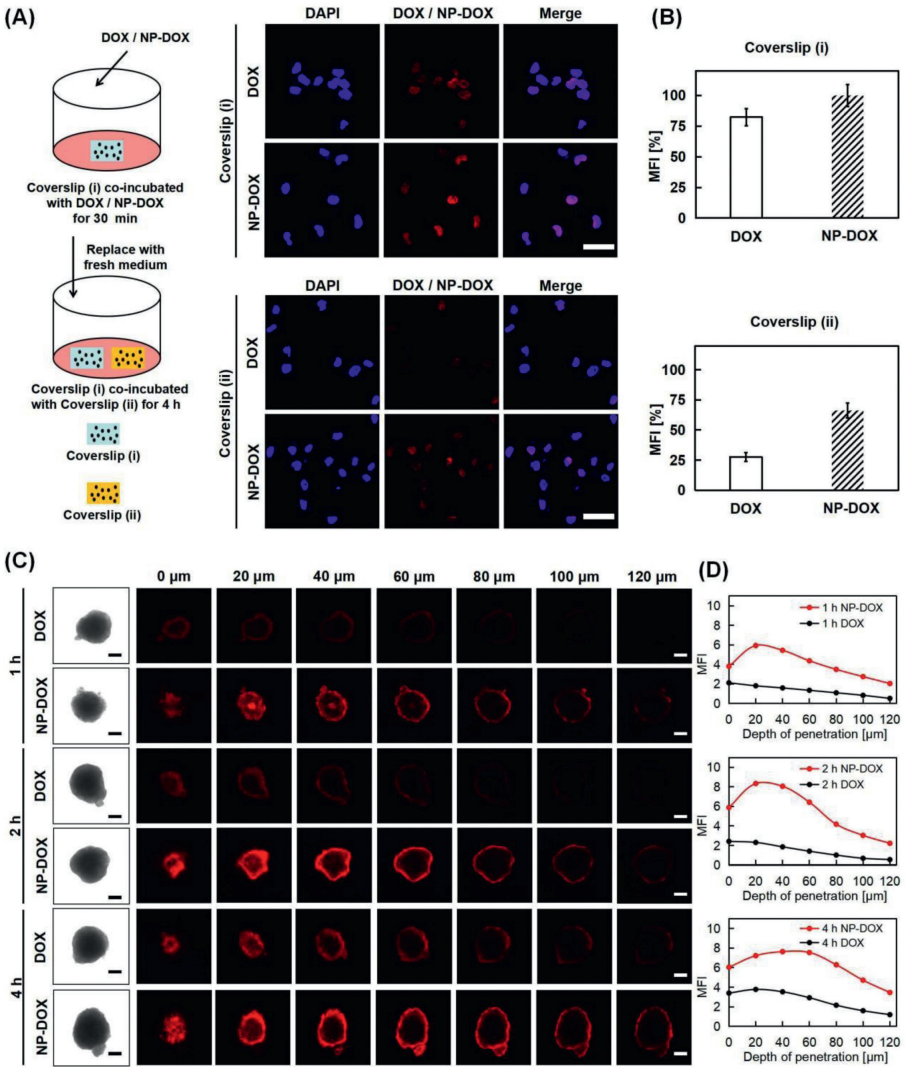

Fig. 3. Intracellular transfer and *in vitro* penetration testing of NP-DOX. (A) CLSM images and (B) analyzed MFI of MDA-MB-231 cells on coverslip (i) and coverslip (ii). Scale bar = 50 μm. Data are presented as means ± standard deviations ($n = 3$). (C) CLSM observations and (D) quantitive analysis of DOX and NP-DOX penetrating the MDA-MB-231 tumor spheroids at 1, 2 and 4 h. Scale bar = 100 μm.

IP3 has been convincingly demonstrated [36–38]. Thus, enzyme-linked immunosorbent assay (ELISA) of IP3 was conducted on MDA-MB-231 cells after 2 h incubation with 50 μg/mL P12. The result in Fig. S10 (Supporting information) demonstrated a 4–5 times increased secretion of IP3 since MDA-MB-231 cells was co-incubated with P12. Although IP3 will not directly release calcium, its binding with IP3 receptors will elevate intracellular calcium by mobilization of calcium store, resulting in a significant increase of intracellular calcium [39].

To study the influence of cationization, tentative exploration was carried out on intracellular transfer of NP-DOX between MDA-MB-231 cells, which was verified to be a Y_1R over-expressed system (Fig. S3 in Supporting information). As visualized in Fig. 3A, DOX had limited transportation between cells. In contrast, the DOX fluorescence intensity from NP-DOX was almost 3-fold higher (Fig. 3B) in the cells on coverslip (ii), which indicated that some NP-DOX internalized by the cells on coverslip (i) was exocytosed and subsequently internalized by the cells on coverslip (ii), achieving efficient transcytosis due to micropinocytosis and positive-charge mediated lysosomal escape.

To seek the possibilities of deep penetration on the basis of being able to achieve effective transcytosis, three-dimensional tumor spheroids were adopted to mimic MDA-MB-231 tumor tissues to evaluate the penetration of NP-DOX. As depicted in Fig. 3C, DOX was restricted on the outer layer of the tumor spheroids after 1 h incubation, which could be easily flushed, leading weaker fluorescence intensity in confocal images. While NP-DOX penetrated deeper into the tumor spheroids, showing stronger and more durable fluorescence (Fig. 3D).

To assess Y_1R targeting of P12, bilateral tumor model was adopted with Y_1R-knock-down MDA-MB-231 cells (left side) and normal MDA-MB-231 cells (right side). All the animal experimental procedures conducted were approved by the Regional Ethics Committee for Animal Experiments at Ningbo University, China (Permit No. SYXK (Zhe) 2019–0005). As shown in Fig. S11 (Supporting information), different tumors exhibited diverse selective accumulation of IR808-labled P12 (NP-IR808) after 12 h injection through the tail vein, clarifying the high binding of P12 to Y_1R highly expressed TNBC tumors *in vivo*. To evaluate the antitumor ability of NP-DOX, weight fluctuations of tumor-bearing mice were frequently utilized as a warning indicator of possible side effects from chemotherapeutic medication. Fig. 4A showed that the body weight of free DOX-treated mice decreased dramatically within 12 days compared to PBS group, indicating unbearable side effects of DOX after the fifth injection. In contrast, there were no significant differences in reasonable growth of body weight between NP-DOX-

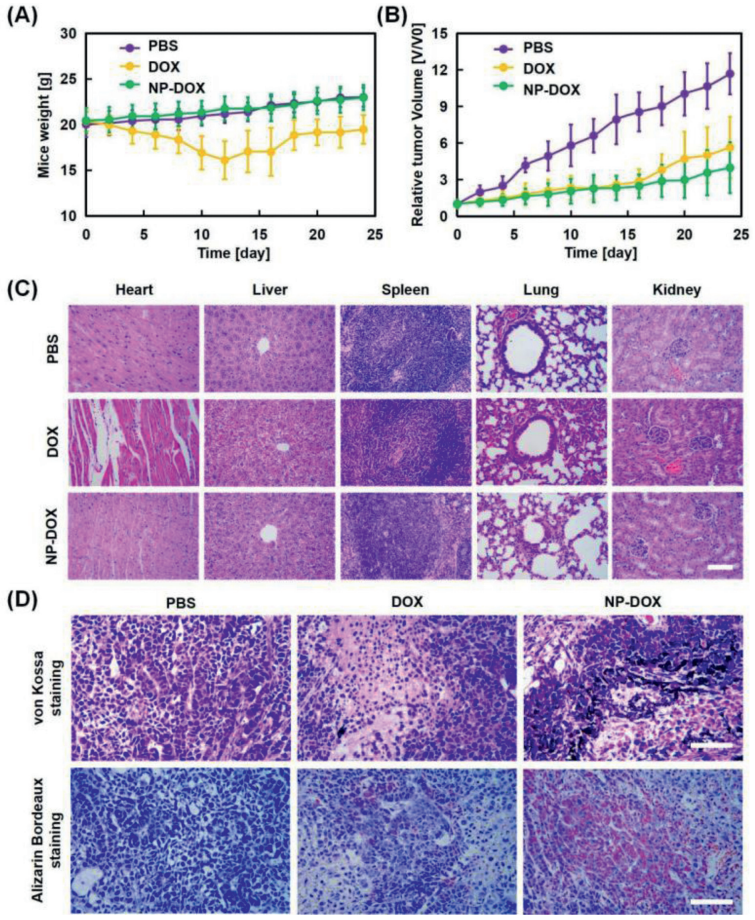

Fig. 4. *In vivo* anticancer activity of NP-DOX in the MDA-MB-231 tumor xenograft model. (A) Weight and (B) tumor volume of tumor-bearing mice in the DOX or NP-DOX-treated group and the control group. Data are presented as means ± standard deviations ($n = 5$). (C) H&E staining of vital organs of MDA-MB-231 tumor-bearing mice after indicated treatments. Scale bar = 200 μm. (D) H&E combined von Kossa (black) or Alizarin Bordeaux staining (magenta) of tumor tissues after indicated treatments. Scale bar = 200 μm.

and PBS-treated groups. As shown in Fig. 4B, the tumor size during the whole treatment period grew rapidly for PBS-treated group, while DOX and NP-DOX showed significant tumor inhibition. Particularly, tumor volume with NP-DOX-treated was nearly 50% and 15% of that with DOX- and PBS-treated. At the end of treatment, all major organs including heart, liver, spleen, lung and kidney and tumor tissue of mice from each group were collected for histopathological analysis. The results of hematoxylin-eosin (H&E) staining in Fig. 4C showed that there were visible morphological and pathological changes in the heart and some decrease in size and number of splenic corpuscles with free DOX, demonstrating toxicity of cardiomyocytes and myelosuppression. However, these side effects were effectively abolished by the conjugate of P12. Evidences were provided that few histopathologic lesions were observed after treatment with NP-DOX. Moreover, calcium deposition of tumor tissues in NP-DOX group was detected *via* von Kossa (black) and Alizarin Bordeaux staining (magenta) in Fig. 4D. In a word, overwhelming advantage was produced by NP-DOX for both safety and effectiveness.

In conclusion, acid-activatable neuropeptide Y analogue-drug conjugate NP-DOX was developed for cancer chemotherapy of Y_1R over-expressed TNBC tumors. Enhanced tumor penetration *in vitro* was successfully achieved due to the covalently attached cationic peptide to DOX. Moreover, Y_1R-mediated promotion of intracellular calcium level *via* second messenger IP3 was discovered, which was confirmed to result in calcium deposition in tumor tissues. Its selective drug release yielded promoted biosafety and tumor suppression *in vivo*. In short, this study demonstrated that NP-DOX is an effective chemotherapeutic agent, which may evoke the development and application of neuropeptide drug conjugates for clinical cancer therapy of Y_1R over-expressed TNBC.

Declaration of competing interest

The authors declare that they have no known competing financial interests or personal relationships that could have appeared to influence the work reported in this paper.

Acknowledgments

This work was financially supported by the Key R&D Program of Zhejiang Province (No. 2020C03110), the National Natural Science Foundation of China (Nos. T2222021, 32011530115, 32025021), the Science & Technology Bureau of Ningbo City (Nos. 2020Z094, 2021Z072) and Excellent Member of Youth Innovation Promotion Association Foundation of CAS (No. Y2021079). Furthermore, the authors genuinely appreciated the help from Yunchao Xia for synthesis of NP-DOX and Ao Xu for PCR analysis.

Supplementary materials

Supplementary material associated with this article can be found, in the online version, at doi:10.1016/j.cclet.2023.108672.

References

[1] M.R. Bruchas, K.S. Girven, L. Mangieri, Trends Neurosci. 45 (2022) 899–912.
[2] A. Schroeder, J.J. Letzkus, Cell 184 (2021) 5501–5503.
[3] E. Yeom, H. Shin, W. Yoo, et al., Nat. Cell Biol. 23 (2021) 172–183.
[4] V.M. Ahrens, K.B. Kostelnik, R. Rennert, et al., J. Control. Release 209 (2015) 170–178.
[5] D. Boehme, J. Krieghoff, A.G. Beck-Sickinger, J. Med. Chem. 59 (2016) 3409–3417.
[6] D.J. Worm, P. Hoppenz, S. Els-Heindl, et al., J. Med. Chem. 63 (2020) 2358–2371.
[7] D. Chakroborty, S. Goswami, H. Fan, et al., Br. J. Cancer 127 (2022) 1440–1449.
[8] M. Alshalalfa, P.L. Nguyen, H. Beltran, et al., Eur. Urol. Oncol. 2 (2019) 405–412.
[9] P. Dietrich, L. Wormser, V. Fritz, et al., J. Clin. Invest. 130 (2020) 2509–2526.
[10] C. Lu, A. Mahajan, S.H. Hong, et al., Nat. Commun. 13 (2022) 2323.
[11] Y. Cheng, X. Tang, Y. Li, et al., Clin. Cancer Res. 25 (2019) 2621–2632.
[12] J. Li, Y. Tian, A. Wu, Regen. Biomater. 2 (2015) 215–219.
[13] C. Morgat, A.K. Mishra, R. Varshney, et al., J. Nucl. Med. 55 (2014) 1650–1657.
[14] B.M. Cooper, J. Iegre, D.H. O' Donovan, M.O. Halvarsson, D.R. Spring, Chem. Soc. Rev. 50 (2021) 1480–1494.
[15] Y. Zhu, K. Tang, J. Lv, Trends Pharmacol. Sci. 42 (2021) 857–869.
[16] L. Salkoff, A. Butler, G. Ferreira, C. Santi, A. Wei, Nat. Rev. Neurosci. 7 (2006) 921–931.
[17] D. Wicher, R. Schaefer, R. Bauernfeind, et al., Nature 452 (2008) 1007–1010.
[18] J. Maynard, S. Okuchi, S. Wastling, et al., Radiology 296 (2020) 111–121.
[19] B. Liu, Y. Bian, S. Liang, et al., ACS Nano 16 (2022) 617–630.
[20] B. Liu, S. Liang, Z. Wang, et al., Adv. Mater. 33 (2021) 2101223.
[21] M. Zhang, R. Song, Y. Liu, et al., Chem 5 (2019) 2171–2182.
[22] P. Zheng, J. Ding, Asian J. Pharm. Sci. 17 (2022) 1–3.
[23] N. Tang, H. Li, L. Zhang, et al., Angew. Chem. Int. Ed. 60 (2021) 6509–6517.
[24] R. Zhao, B. Wang, X. Yang, et al., Angew. Chem. Int. Ed. 55 (2016) 5225–5229.
[25] Y. Liu, Z. Jiang, S. Tong, et al., Adv. Mater. 35 (2022) e2203291.
[26] J.C. Wu, Y.N. Chen, J.X. Xin, et al., Adv. Funct. Mater. 31 (2021) 2101284.
[27] Z. Jiang, Y. Liu, R. Shi, et al., Adv. Mater. 34 (2022) e2110094.
[28] L. Dong, J. Ding, L. Zhu, et al., Chin. Chem. Lett. 34 (2023) 108192.
[29] J. Chen, Z. Jiang, Y.S. Zhang, J. Ding, X. Chen, Appl. Phys. Rev. 8 (2021) 041321.
[30] J. Chen, J. Yang, J. Ding, J. Mater. Chem. B 10 (2022) 7173–7182.
[31] X. Feng, W. Xu, X. Xu, et al., Sci. China Chem. 64 (2021) 293–301.
[32] J. Huotari, A. Helenius, EMBO J. 30 (2011) 3481–3500.
[33] K. Xiao, Y. Li, J. Luo, et al., Biomaterials 32 (2011) 3435–3446.
[34] Y. Ning, L. Wei, S. Lin, et al., Chin. Chem. Lett. 33 (2022) 4710–4714.
[35] M. Cong, G. Xu, S. Yang, et al., Chin. Chem. Lett. 33 (2022) 2481–2485.
[36] A.J. Daniels, O.H. Viveros, J.E. Matthews, Mol. Cell. Neurosci. 5 (1994) 466–474.
[37] H. Herzog, Y.J. Hort, H.J. Ball, et al., Proc. Natl. Acad. Sci. U. S. A. 89 (1992) 5794–5798.
[38] M.C. Michel, Trends Pharmacol. Sci. 12 (1991) 389–394.
[39] R. Rizzuto, P. Pinton, W. Carrington, et al., Science 280 (1998) 1763–1766.